JOURNAL OF CATALYSIS **171,** 191–207 (1997)
ARTICLE NO. CA971761

Crystallization Behavior of Tungstate on Zirconia and Its Relationship to Acidic Properties

I. Effect of Preparation Parameters

Raymond A. Boyse and Edmond I. Ko[1]

Department of Chemical Engineering, Carnegie Mellon University, Pittsburgh, Pennsylvania 15213-3890

Received February 26, 1997; revised June 2, 1997; accepted June 3, 1997

Zirconia-tungstate aerogels were prepared by two methods, a one-step sol–gel synthesis and an incipient wetness impregnation. The effects of preparation parameters on their physical and chemical properties were studied. The catalytic activity and surface acidity were characterized by a set of chemical probes, including *n*-butane isomerization and pyridine adsorption, which were developed into an acidity scale for the evaluation of solid acids in general. Maximum catalytic activity in *n*-butane isomerization occurred at saturation monolayer coverage of zirconia by tungstate. The one-step synthesis required a more elevated activation temperature in order to expel tungstate from the bulk of zirconia before dispersion on the surface. Variation of the activation temperature allowed study of the transition between a catalytically inactive and active material and consequently identification of the active species. Activity in *n*-butane isomerization coincided with the presence of (i) a larger population of Brønsted sites and (ii) stronger Brønsted sites on the surface. Infrared spectroscopy indicated that the surface active tungstate species was identical regardless of preparative route. We conclude that the preparation method affected the activation behavior of zirconia-tungstate materials but not the active species in *n*-butane isomerization. Furthermore, zirconia-tungstate can be placed in a meaningful Brønsted acid strength scale which has the potential as a tool for ranking acid catalysts.

INTRODUCTION

Solid acid catalysts play an important role in hydrocarbon conversion reactions in the chemical and petroleum industries (1, 2). An emerging class of materials is that of oxides, such as zirconia, modified by anions, such as sulfate (3–7) or phosphate (8), to yield solid acids of a wide range of strengths. Anionic dopants create additional electron deficient regions that increase the Brønsted acid strength of a metal oxide surface by improving the ability of neighboring hydroxyl groups to act as proton donors (1, 2). The strong acidity of zirconia-supported sulfate attracted much attention because of its ability to catalyze a range of reactions such as cracking, alkylation, and isomerization. The potential for a heterogeneous catalyst, with a reduced environmental risk compared to conventional halogen-based catalysts, has yielded many reports on the activity of zirconia-sulfate based materials (3–7). Recently, Hino and Arata reported zirconia-supported tungstate as an alternative material in reactions requiring strong acid sites (9, 10). They demonstrated the effectiveness of this material in the skeletal isomerization of *n*-butane at low temperatures, a reaction of particular interest in the production of octane-enhancing additives to gasoline. Several advantages of tungstate, over sulfate, as dopant include that it does not suffer from dopant loss during thermal treatment and it undergoes significantly less deactivation during catalytic reaction (11, 12). It has also been shown that zirconia-tungstate promoted with platinum has superior selectivity in isomerizations of larger alkanes such as *n*-heptane (11, 13).

Considerable study to date has provided a reasonable description of zirconia-tungstate as a solid acid catalyst (9–14). With sufficient heat treatment, solid–solid wetting of zirconia by tungstate stabilizes textural and structural properties against sintering. These materials are catalytically active at near saturation monolayer coverage of zirconia by tungstate after calcination in the range 1073 to 1123 K (9–11). By comparison to tungstate promoted onto alumina (15), titania (16), and silica (17), it has been established that dispersed tungsten oxide species on zirconia form distorted octahedrally coordinated surface polytungstate species under dehydrated conditions. Optimum activation enhances the Brønsted acidity compared to other modified oxides (18) or modified crystalline zirconia (10, 19). But there are questions that remain unanswered such as what is the active species in alkane isomerization and what is the relationship between surface acidity and catalytic activity.

In this work, we wish to understand the relative importance of preparative variables on the acidic and catalytic

[1] To whom correspondence should be addressed. Fax: 412-268-7139. E-mail: edko@cmu.edu.

0021-9517/97 $25.00

properties of zirconia-tungstate. Previous reports have stated that only the chemical nature of the support and the active oxide are important to the catalytic activity of a material (20, 21). Synthesis was suggested not to be crucial since it could not influence the structure of the final supported oxide. Hino and Arata reported that the catalytic properties depend greatly on the calcination temperature of the zirconium hydroxide before dopant promotion (10). Zhao *et al*. (19) reported similar results in relation to strong acidic properties. Afanasiev *et al*. (22) concluded, from a set of zirconia-tungstate materials prepared using molten salts, that the preparation method appears to strongly influence the state of the tungstate species (22). Therefore, it seems that several factors—such as the method of tungstate incorporation, the activation temperature, and even the chemical precursors—may play important roles in the formation of zirconia-tungstate solid acids.

By understanding the relationship between acidity and catalytic activity, we also wish to develop an acidity scale that can qualitatively describe the acidity of zirconia-tungstate and allow comparison to other materials. A number of techniques have been employed to characterize zirconia-sulfate. Kustov *et al*. (6) and Adeeva *et al*. (7) determined the acid strength of zirconia-sulfate by the shift in the infrared signature of the O−H species before and after the adsorption of weak bases to show that the strength of Brønsted sites is not enhanced. Venkatesh *et al*. (5) used the cleavage of diphenylmethane (a Brønsted-acid catalyzed reaction) to demonstrate the existence of stronger Brønsted acid sites after sulfate promotion. Previous work by Ramis *et al*. (23) has compared titanias doped with sulfate, tungstate, and phosphate in olefin oligomerizations. In doing so, they have ranked the acidities of anion doped titania and shown how a set of well-selected reactions can be used to classify the acid quality. Miller and Ko (24) have used a combination of chemical probes, the isomerization of *n*-butane and 1-butene in conjunction with pyridine adsorption, to distinguish between the maximum Brønsted acid strength of zirconia-silica-sulfate aerogels. We have used the same techniques in this study to characterize the maximum Brønsted site strengths on zirconia-tungstate and expanded this acidity scale further to allow a more meaningful description of solid acid materials. We believe that placement of the doped zirconias in a matrix or hierarchy that ranks Brønsted acid strength is a step toward developing a tool for preparing solid acids, by design, with controlled site density and strengths for a given application.

EXPERIMENTAL

Sample Preparation

Zirconia-tungstate aerogels were prepared by two methods: an incipient wetness impregnation and a one-step preparation. The sol–gel parameters used in preparing the aerogels are summarized in Table 1. The material delivered by the incipient wetness preparation (IWP) required an undoped zirconia aerogel onto which tungstate could be placed. The starting synthetic formulation is described elsewhere (25). Briefly, we added 16.2 ml zirconium *n*-propoxide (70 wt% in propanol, Alfa) to a solution of 15 ml 1-propanol (Fisher) and 1.91 ml HNO_3 (70% w/w, Fisher). In a second beaker, 1.31 ml distilled water was mixed with 15 ml 1-propanol. The contents of the second beaker were rapidly added to the solution in the first beaker which was stirred by a magnetic stir bar until gelation occurred. The gelation point was recognized with the disappearance of the vortex caused by stirring. The exact time between mixing and gelation was recorded in Table 1 as the gel time. The product alcogel was aged for 2 h at room temperature before displacement of the alcohol solvent by carbon dioxide under supercritical conditions. In an autoclave (Autoclave Engineers, model 08U-06-60FS) operating at about 343 K, 20×10^3 kPa, with a downstream CO_2 flowrate of 85 liters/h at ambient conditions, the alcohol was displaced from the alcogel in approximately 2 h. The product aerogel was ground into a powder to pass through 100 mesh. Subsequent drying consisted of heating at 383 K under a vacuum of 3.4 kPa for 3 h to remove water, followed by heating at 523 K under vacuum for 3 h to remove residual organics and nitrates. Tungstate (10 wt% W, nominal) was incorporated by impregnation to incipient wetness of the X-ray amorphous powder with an aqueous solution of ammonium metatungstate hydrate (Aldrich). The material was then dried under vacuum at 383 K for 3 h followed by calcination in flowing oxygen (27 liters/h) for 2 h at a temperature in the range 973 to 1273 K, referred to as the activation temperature. We denote this material, with surface tungstate, as IWP-10.

TABLE 1

Sol–Gel Parameters for the Preparation of Zirconia-Tungstate Aerogels[a]

Sample	Solvent	Gel time (s)	Water content (ml)	Acid content (ml)	Hydrolysis ratio (mol H_2O/mol Zr)	Acid ratio (mol HNO_3/mol Zr)
Co-18	Ethanol	83	2.62	2.55	5.00	0.754
Co-10	Ethanol	49	2.62	2.50	4.98	0.738
IWP-18	Ethanol	34	2.62	2.40	4.95	0.710
IWP-10	Propanol	48	1.31	1.91	2.78	0.562

[a] All gels prepared in 30 ml alcohol.

The second method of preparation of zirconia-tungstate aerogels was a one-step preparation in which tungstate was introduced directly in the gelling step. The preparation was based on that for an undoped zirconia aerogel (25). To ensure solubility of the tungstate precursor, the one-step

preparation involved changing the solvent from 1-propanol to ethanol and increasing the acid content. The water content was increased accordingly to promote gelation. Briefly, we added 16.2 ml zirconium *n*-propoxide to a solution containing ammonium metatungstate dissolved in 15 ml ethanol (dehydrated 200 proof, pharmco) and HNO_3. In a second beaker, distilled water was mixed with 15 ml ethanol. The ammonium metatungstate contents were calculated to yield nominal loadings of 10 and 18 wt% W. The water and acid amounts corresponding to each tungstate loading are given in Table 1. After aging for 2 h, the product alcogels were supercritically dried with CO_2 and ground into a powder. The aerogels were sequentially dried under vacuum at 383 and 523 K for 3 h, followed by calcination in flowing oxygen at a temperature in the range 973 to 1273 K. The two samples delivered by this preparation with 10 and 18 wt% W, throughout the bulk of zirconia, were defined as co-gels and labeled Co-10 and Co-18, respectively.

To understand the relative importance of the sol–gel parameters on the final properties of the aerogels, a second material was prepared by the incipient wetness impregnation of a zirconia support that had been prepared with parameters matching the one-step preparation. The procedure followed was identical to that used to deliver the impregnated aerogel with 10 wt% W labeled IWP-10. The solvent used was changed to ethanol while the water and acid contents were increased to match those of the co-gels. The amounts of each component are given in Table 1. The tungstate loading was increased to 18 wt% W delivering a material labeled as IWP-18.

Sample Characterization

Textural characterization was determined by nitrogen adsorption/desorption using an Autosorb-1 gas sorption system (Quantachrome Corp.). Samples were outgassed at 383 K, under vacuum for 2 h prior to analysis. Forty point desorption isotherms were obtained, from which the BET surface area (taken at $P/P_0 \cong 0.3$), total pore volume (at P/P_0 close to unity), and pore size distribution (BJH method) were calculated. Identification of crystal phase was made from X-ray powder diffraction (XRD) patterns obtained using a Rigaku D/max diffractometer with Cu Kα radiation. The phase identification of tungsten oxide was further examined using Raman spectroscopy. Laser Raman spectra were recorded using a Spex 1403 0.85-m double spectrometer. The 488-nm line of a Spectra-Physics model 2020 Argon ion laser, with a power output of about 200 mW, was used for excitation. Spectra were gathered from stationary samples contained in glass vials, under ambient conditions, over the range 200 to 1200 cm^{-1} with a spectral slit width of 600 μm and a step size of 2 cm^{-1}. Previous work with supported tungstate has shown that the most prominent Raman bands are from the W–O vibrations of crystalline WO_3 at 805, 715, 250 cm^{-1} by which the crystallization of tungsten oxide can be monitored. Raman bands from 960–980 cm^{-1} are associated with W=O vibrations of hydrated polytungstate species on zirconia (20). Finally, bands at 1010 cm^{-1} are assigned to a dehydrated two-dimensional octahedrally coordinated surface species (20).

Catalytic activities were determined using a differential, downward flow, tubular fixed-bed reactor of 12.7 mm diameter. Approximately 0.5 g of sample was pretreated at 588 K for 1 h under 2.4 liters/h (40 sccm) flowing helium. The sample was then cooled to 553 K and exposed to a feed stream mixture of 0.06 liters/h (1 sccm) *n*-butane (Matheson, Research Grade) in 0.60 liters/h (10 sccm) hydrogen (Matheson UHP). A Gow–Mac 550P gas chromatograph with thermal conductivity detector (Column: Supelco 23% SP 1700 on 80/20 Chromosorb, 1/8 in. $\times$ 30 ft) was used to determine the composition of the product stream.

Diffuse reflectance infrared Fourier transform (DRIFT) spectroscopy was employed to characterize the state of the tungstate species on the materials and the acidity associated with these species. The experiments were carried out on a Mattson Galaxy 5020 FTIR, with a DTGS detector and a Harrick diffuse reflectance attachment (DRA-2). Additionally, *in situ* DRIFT spectroscopy was performed using a Harrick reaction chamber (HVC-DR2). Each spectrum was obtained by averaging 128 scans taken over the range 400–4000 cm^{-1} at a resolution of 2 cm^{-1}. *Ex situ* and *in situ* DRIFT spectra were obtained from samples diluted to 5 wt% in KBr. *Ex situ* spectra were acquired under ambient conditions, while *in situ* DRIFT spectra were acquired under flowing helium at about 2.4 liters/h. Under *in situ* conditions, samples were pretreated at 588 K for 15 min after which a spectrum was gathered under conditions similar to those used in the isomerization of *n*-butane. To measure the type and strength of acidity on the surface, the samples were cooled to 373 K and subsequently exposed to pyridine for 15 min by diverting the helium flow through a pyridine saturator. Spectra were then taken at 373, 423, 473, 553, and 623 K after 10 min in flowing helium at each temperature. All spectra were obtained using a KBr reference spectrum, obtained in helium at room temperature, to determine the absorbance by the samples. Preliminary testing using KBr reference spectra obtained at higher temperatures did not show any new features. The *type* of surface acidity was determined by the peaks at 1445 and 1490 cm^{-1}—the former peak is caused by the presence of coordinately bound pyridine on Lewis acid sites and the latter by pyridine irreversibly adsorbed on both Brønsted and Lewis acid sites (26). Relative populations of Brønsted and Lewis sites were calculated by the method of Basila and Kantner (27) using the integrated areas under the above-mentioned peaks. A reference aerogel, with Lewis acid sites only, was used to determine the relative contribution of coordinately bound pyridine to the areas under the 1445 and 1490 cm^{-1} peaks. The percentages of Brønsted acid sites were measured for samples heated at

473 K to avoid problems with physisorbed pyridine at low temperatures and uncertainties with peak analysis at higher temperatures due to thermal noise. The relative *strength* of the acid sites was determined by monitoring the effect of temperature on the peaks at 1445 and 1490 cm^{-1}. Materials with stronger Brønsted acid sites retained irreversibly adsorbed pyridine up to higher temperatures.

RESULTS

Textural Properties of Zirconia-Tungstate Aerogels

The effect of preparation on the textural properties of zirconia-tungstate aerogels was studied. For each preparative route, we examined the role of (i) final activation temperature, (ii) tungstate loading, and (iii) sol–gel parameters. The effect of activation temperature on the surface areas and pore volumes of the aerogels can be seen in Table 2. After calcination at 1073 K, the BET surface areas were in the range 56 to 73 m^2/g. These areas were higher than those of previously reported zirconia-tungstate materials (9–11), and considerably higher than that of a pure zirconia aerogel (25). The increase in surface area was attributed to the inhibition of sintering by the presence of a dopant (4, 8). The role of sintering, shown in Fig. 1 for Co-10 and IWP-10, was apparent by a constant loss in surface area with increasing activation temperature. The presence of tungstate on the surface of IWP-10 and in the bulk of Co-10 appeared to stabilize the surface areas to a similar extent. The role of tungstate loading was evident by comparing two co-gels with 10 and 18 wt% W. Table 2 shows that, after activation at 1073 K, Co-10 and Co-18 have similar surface areas and pore volumes. Recall that these two gels were prepared with nearly identical sol–gel parameters. Apparently under these conditions, tungstate loading at the level used in this study did not change the gel network appreciably.

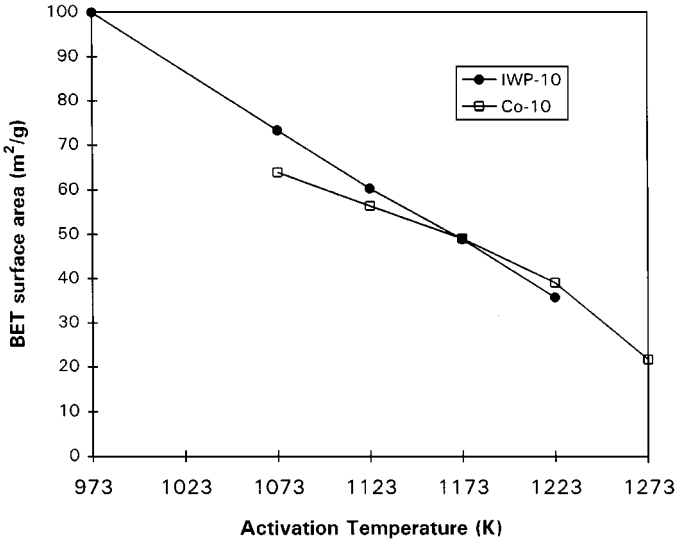

FIG. 1. Effect of heat treatment (calcination at indicated temperature for 2 h) on the BET surface areas of impregnated aerogel and co-gel with 10 wt% W nominal loading (IWP-10 and Co-10, respectively).

Variation of certain sol–gel parameters was necessary in order to prepare materials by two preparative routes, the effect of which was evidenced in the textural properties. The parameters changed were hydrolysis ratio, acid ratio, and choice of solvent. Comparing Co-10 and IWP-10 activated at 1073 K, we observed a difference in the surface areas, 64 and 73 m^2/g, respectively, and in the pore volumes, 0.57 and 0.33 cm^3/g, respectively. The large difference in pore structure was further illustrated by the pore size distributions shown in Figs. 2 and 3. Co-10 had a broader distribution of pores with radii centered around 15 nm in contrast to IWP-10 which had a narrow distribution centered around 8 nm. It was noted that Co-10 and IWP-10 had different sets of sol–gel parameters in addition to being prepared by different methods. To elucidate the relative importance of each sol–gel parameter and the preparative route, we studied the role of preparation method by comparing co-gels and an impregnated aerogel with similar sol–gel parameters. Table 1 shows that IWP-18, Co-18, and Co-10 had near identical sol–gel parameters but that after calcination at 1073 K, the pore volume of IWP-18 (0.45 cm^3/g) was less than those of the co-gels (0.57 cm^3/g and 0.55 cm^3/g). This observation verified that changing the preparation method, and thus the location of the dopant in the aerogel, resulted

TABLE 2

Textural Properties of Zirconia-Tungstate Aerogels

Sample	Activation temperature (K)	Nominal loading (wt% W)	Nominal loading[a] (W/nm^2)	Pore volume (cm^3/g)	Surface area (m^2/g)
Co-10	1073	10	N/A[b]	0.57	63.9
	1173	10		0.56	56.4
	1223	10		0.53	49.1
	1273	10		0.41	39.1
IWP-10	973	10	3.6	0.33	100.0
	1073	10	5.0	0.33	73.2
	1123	10	6.0	0.33	60.3
	1173	10	7.4	0.31	48.9
	1223	10	10.4	0.27	35.8
Co-18	973	18	N/A[b]	0.55	89.2
	1073	18		0.55	67.7
	1123	18		0.53	57.2
	1173	18		0.50	46.6
	1223	18		0.38	34.2
IWP-18	1073	18	12.8	0.45	56.1
	1123	18	14.9	0.43	48.3
	1173	18	18.8	0.41	38.2

[a] Calculation based on the experimentally determined BET surface areas and assuming each W-unit occupied a surface area of 0.16 nm^2.

[b] Not available as surface loading was unknown due to the method of preparation.

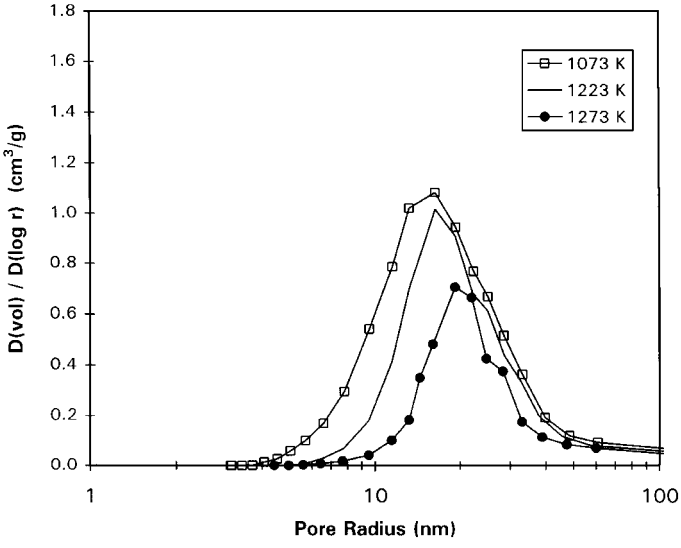

FIG. 2. Effect of heat treatment on the pore size distribution, as determined from nitrogen desorption, for co-gel with 10 wt% W (Co-10).

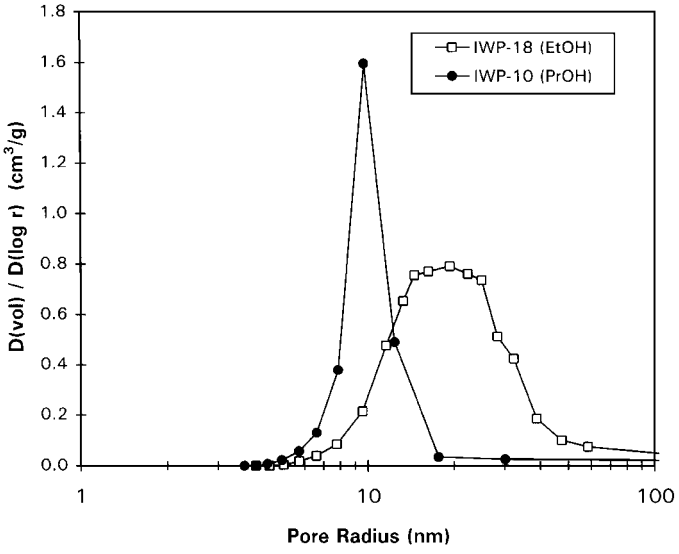

FIG. 4. Effect of tungstate loading and choice of alcogel solvent on the pore size distributions of impregnated aerogels, calcined at 1173 K for 2 h in flowing oxygen.

in a moderate increase in pore volume. However, Fig. 4 shows that aerogels prepared by the same method, IWP-10 and IWP-18, had substantially different pore size distributions. Hence, although pore volume was affected by the location of the dopant in the aerogel, the marked shift in pore size distributions could *not* be attributed to different preparation methods. The difference between the two impregnated aerogels was therefore a result of a change in sol–gel parameters, namely the hydrolysis ratio, acid ratio, and the choice of solvent. Since the gel times of the supports for the impregnated aerogels were similar, as shown in Table 1, the higher acid and water ratios should not have substantially altered the average pore size (25). Hence, we believe the change of solvent played the most significant role in controlling the pore structure.

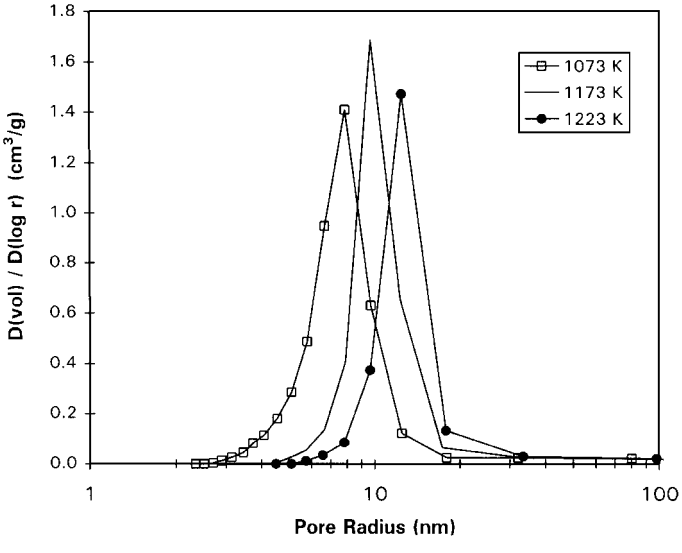

FIG. 3. Effect of heat treatment on the pore size distribution, as determined from nitrogen desorption, for impregnated aerogel with 10 wt% (IWP-10).

Structural Properties of Zirconia-Tungstate Aerogels

The identification of zirconia and tungsten oxide phases was made using X-ray diffraction. Pure zirconia aerogels transform into a metastable tetragonal phase with activation at 773 K and into a monoclinic phase with activation at 1173 K (25). Figure 5 shows the X-ray diffraction patterns for each of the zirconia-tungstate aerogels over the range of activation temperatures. The tetragonal phase was evident for all of the samples with calcination at 1173 K, illustrating the inhibition of the sintering of zirconia by the presence of a dopant. The tetragonal-to-monoclinic transformation was retarded by the addition of tungstate, up to temperatures of 1223 K for the co-gels and 1173 K for the impregnated aerogels.

Figure 5 illustrates the role of both the preparative method and the tungstate loading on the formation of crystalline tungsten oxide (WO_3) on the surface of zirconia. The emergence of crystalline WO_3 with increasing activation temperature was identified by three peaks in the X-ray diffraction pattern in the range $2\theta \cong 23$–25°. Comparison of the X-ray patterns of IWP-10 and Co-10 demonstrated the relationship between the preparation method and WO_3 crystallization due to increasing the activation temperature. As the surface area decreased, due to sintering of the underlying zirconia, the tungstate surface concentration on IWP-10 increased, allowing WO_3 formation with activation between 1123–1173 K. The surface

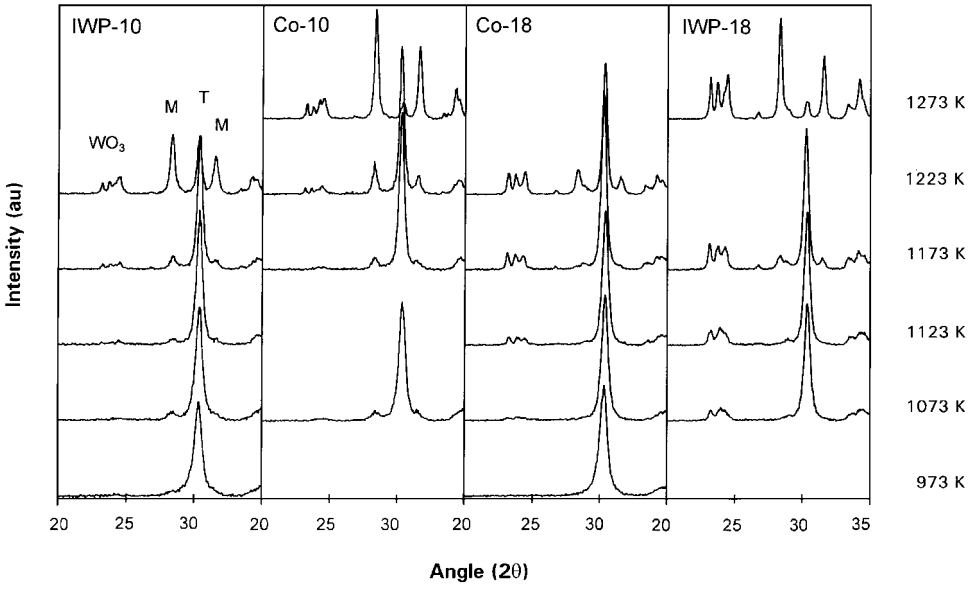

FIG. 5. X-ray diffraction patterns of the co-gels and impregnated aerogels as functions of tungstate loading and activation temperatures. Metastable tetragonal (T) zirconia indexed by a peak at $2\theta = 30^\circ$, crystalline WO_3 by peaks at $2\theta \cong 23$–25°.

concentration was calculated using the experimentally determined BET surface areas and assuming that each W-unit in the layer occupied 0.16 nm^2 (28). At the point when crystalline WO_3 was detected by XRD, the surface tungstate concentration that would correspond to a theoretical monolayer was calculated to be 6.25 W-atoms/nm^2. The onset of crystallization occurred at saturation monolayer coverage of zirconia by tungstate when dispersed tungstate transformed into nanoscale WO_3 crystallites. The presence of WO_3 was not detected on Co-10 until activation between 1173–1223 K. The transformation was delayed to a higher activation temperature because tungstate entrapped in the bulk of the aerogel had to be expelled onto the surface. This behavior has been observed with other doped-zirconia aerogels prepared by a one-step method (4, 8). Crystallization of WO_3 on Co-18 and IWP-18 occurred in the ranges 1073–1123 K and 973–1073 K, respectively. The higher tungstate loadings in samples Co-18 and IWP-18 resulted in the saturation capacity of tungstate being attained on materials of higher surface area and thus at lower activation temperatures. The formation of WO_3 was retarded to a higher temperature in Co-18, relative to IWP-18, because the tungstate first needed to be expelled from the bulk of the aerogel as was the case in Co-10.

The crystal phase of tungstate on zirconia was also examined using Raman spectroscopy. Figures 6 and 7 show the Raman spectra for Co-10 and IWP-10, respectively. The appearance of peaks at 805 and 715 cm^{-1} in the Raman patterns for Co-10 indicated the emergence of WO_3 crystallites on zirconia with activation between 1173–1223 K. This matched the temperature range in which crystalline WO_3 was detected by X-ray diffraction, even though Raman spectroscopy is known to be sensitive to smaller crystallites than XRD (29). Raman spectra of IWP-10 in Fig. 7 showed the existence of WO_3 crystallites between 1073–1123 K which was lower than the activation temperature needed for WO_3 detection by XRD. The crystallization behavior of tungsten oxide ascertained by X-ray diffraction and Raman spectroscopy is summarized in Table 3. It shows that the crystallization of tungsten oxide on Co-10 was detected by both techniques in the same temperature range. The simultaneous detection suggested that the crystallization of WO_3 on Co-10 was more abrupt than on IWP-10. Hence tungstate, expelled from the bulk of zirconia, was

TABLE 3

Tungsten Oxide Crystallization on Zirconia-Tungstate Aerogels

Sample	Temperature range of WO_3 crystallization by XRD	Temperature range of WO_3 crystallization by Raman[a]	Surface tungsten loading (W/nm^2) at WO_3 crystallization[c]
IWP-10	1123–1173	1073–1123	5.0–7.4
IWP-18	973–1073	N/A[b]	<12.8
Co-10	1173–1223	1173–1223	N/A[d]
Co-18	1073–1123	N/A[b]	N/A[d]

[a] Raman spectra obtained from aerogels under ambient conditions.
[b] Not available.
[c] Calculation based on the BET surface areas at activation temperatures of WO_3 crystallization as observed by XRD and Raman spectroscopy. Assume each W-unit occupied a surface area of 0.16 nm^2.
[d] Not available as surface loading was unknown due to the method of preparation.

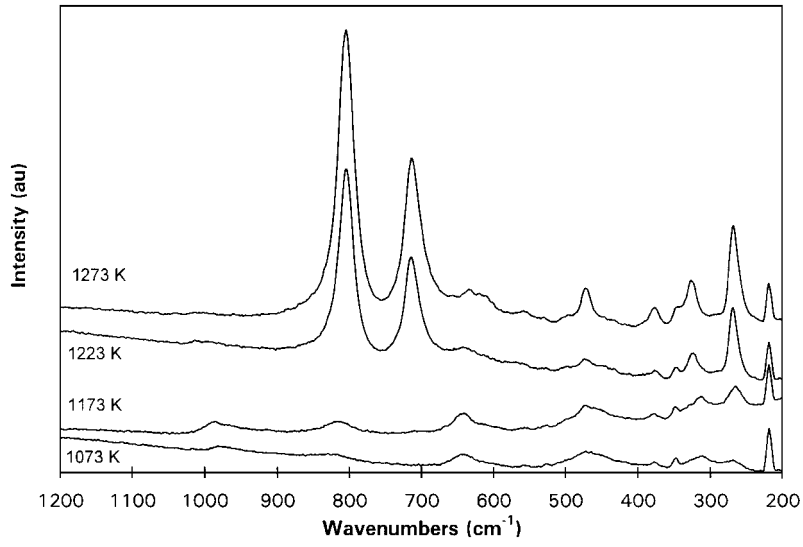

FIG. 6. Raman spectra for the co-gel, with 10 wt% W (Co-10), over a range of activation temperatures. Peaks at 805 and 715 cm^{-1} are indexed to crystalline WO_3.

dispersed on the surface and rapidly crystallized into WO_3 over a small temperature range.

Catalytic Properties of Zirconia-Tungstate Aerogels

The zirconia-tungstate aerogels were probed for strong acid sites by the isomerization of *n*-butane in H_2 at 588 K. Calcination temperatures reported for maximum activity in this reaction are in the range 1073–1123 K (9–12). The performance of the aerogels in this reaction was investigated with respect to tungstate loading, activation temperature, and preparative route. The reaction rates were normalized by the measured catalyst surface area at each activation temperature to allow qualitative comparison between the aerogels. The effect of the activation temperature on the catalytic activity was studied for each of the aerogels. The activity of Co-10, over a 100 min time period, is shown in Fig. 8 and was representative of all of the aerogels. The activity was constant with time-on-stream over the examined time period. This behavior contrasted with zirconia-sulfate aerogels which deactivate substantially in the same time period (4). While the exact mechanism of deactivation on zirconia-sulfate is unclear, the apparent stability of zirconia-tungstate against deactivation compared to zirconia-sulfate was likely due to the resistance of tungstate to decomposition during (i) heat treatments and (ii) reaction in a reducing atmosphere. The profile of steady-state activities over

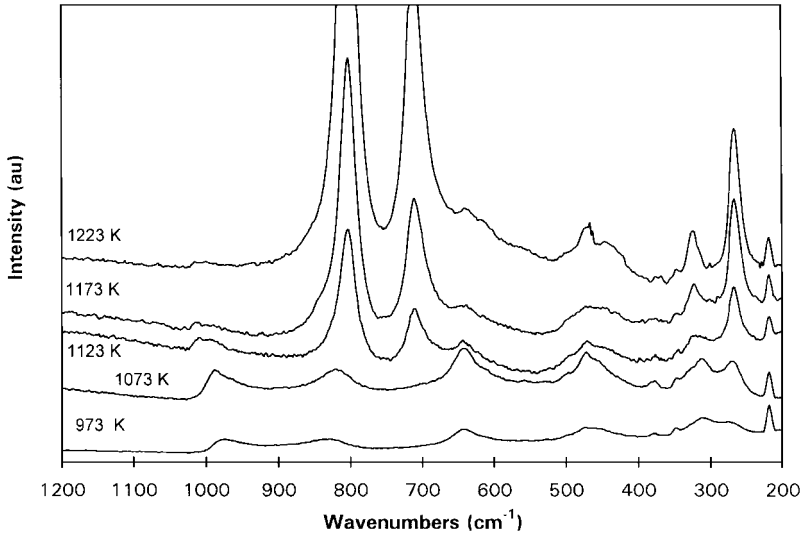

FIG. 7. Raman spectra for the impregnated aerogel, with 10 wt% W (IWP-10), over a range of activation temperatures. Peaks at 805 and 715 cm^{-1} are indexed to crystalline WO_3.

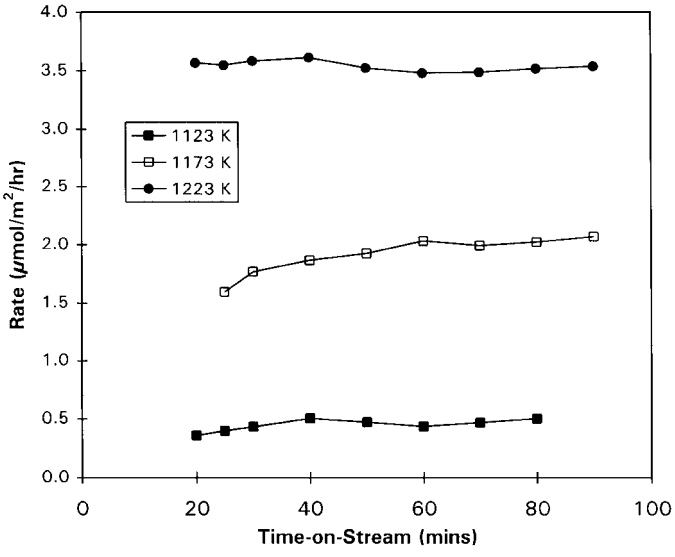

FIG. 8. *n*-butane isomerization rates with time-on-stream for the co-gel with 10 wt% W (Co-10) at different activation temperatures.

the range of activation temperatures is shown in Fig. 9. Maximum activity of IWP-10 was observed after calcination at 1123 K. Since crystalline WO_3 emerged with activation above this temperature, it is possible that the sample activated at 1173 K was more active than that at 1123 K, if the reaction data were normalized by active species. The optimum activation temperature range of 1123–1173 K was slightly higher than those reported by other researchers.

Increasing the loading to 18 wt% W had a detrimental affect on the activity as seen by the activity profile of IWP-18 in Fig. 9. Crystalline WO_3 was present at all of the activation temperatures studied and appeared to cover the surface of zirconia. This resulted in less active species per measured surface area of IWP-18 available for participation in the isomerization of *n*-butane. Hence, the activity, which was in terms of the total surface area, appeared low. The effect of the preparative route on the activity in *n*-butane isomerization was evident by comparing materials Co-10 and IWP-10. Maximum activity for Co-10 occurred at the much higher temperature of 1223 K. This activation temperature was also the temperature at which crystalline WO_3 was first evident and was the highest temperature at which the tetragonal structure of zirconia was stabilized. Activation at 1273 K generated an inactive catalyst consisting predominantly of monoclinic zirconia and crystalline WO_3. The narrow temperature window in which Co-10 was active in this reaction was probably caused by the rapid crystallization of WO_3 after tungstate was expelled from the bulk of the material. The high activation temperature required by Co-10 in comparison to IWP-10 supported the results indicating that tungstate must first be expelled from the bulk before decomposing into a surface active species.

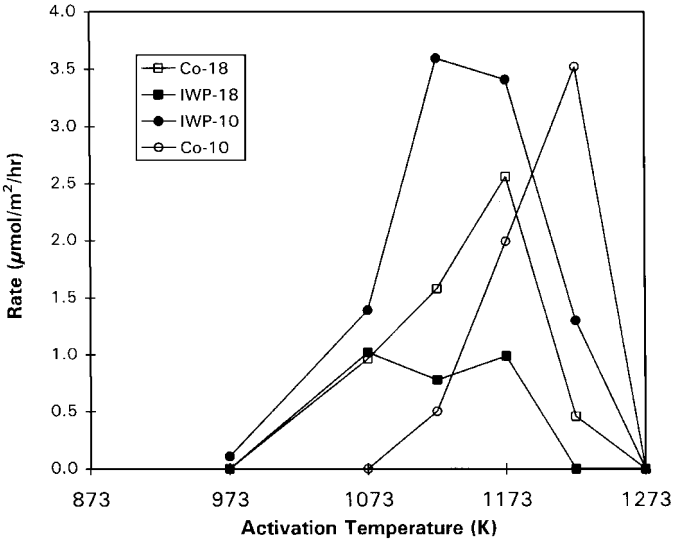

FIG. 9. Effect of activation temperature on steady-state activity (after 70 min time-on-stream) for co-gels and impregnated aerogels with 10 and 18 wt% W. Samples were calcined in flowing oxygen for 2 h at the temperatures indicated.

Acidic Properties of Zirconia-Tungstate Aerogels

The acidic properties of zirconia-tungstate were studied to identify the relationship between catalytic activity and the acidity of the aerogels. We used DRIFT spectra of adsorbed pyridine to determine (i) the *types* of acid sites present on the aerogels and (ii) the relative *strengths* of these acid sites. Previous studies attest that zirconia-tungstate, activated at 1023 K, possesses Brønsted and Lewis acid sites, in contrast to pure zirconia which has Lewis acid sites only and can irreversibly adsorb pyridine up to temperatures of 673 K (18).

Figures 10 and 11 show the DRIFT spectra of adsorbed pyridine on Co-10 activated at 1073 and 1223 K which were inactive and active in the isomerization of *n*-butane, respectively. For the inactive co-gel shown in Fig. 10, the existence of Lewis acid sites was evident by peaks at 1610 and 1447 cm^{-1}. Similarly, Brønsted acid sites were evident by peaks at 1640, 1540, and 1490 cm^{-1}. Physisorbed pyridine was observed on samples heated at 373 and 423 K by a peak at 1575 cm^{-1} which disappeared at temperatures above 423 K. The evolution of the pyridine infrared bands with temperature showed that Brønsted and Lewis acid sites were present up to 553 K. At 623 K, the band at 1490 cm^{-1} corresponding to Brønsted acid sites was too small to detect in background noise, while the bands representing Lewis acid sites were still present at 673 K.

Figure 11 shows the corresponding pyridine DRIFT spectra for the *n*-butane active co-gel activated at 1223 K. It shows the existence of Lewis acid sites, by peaks at 1610 and 1447 cm^{-1}, and Brønsted acid sites, by peaks and 1540

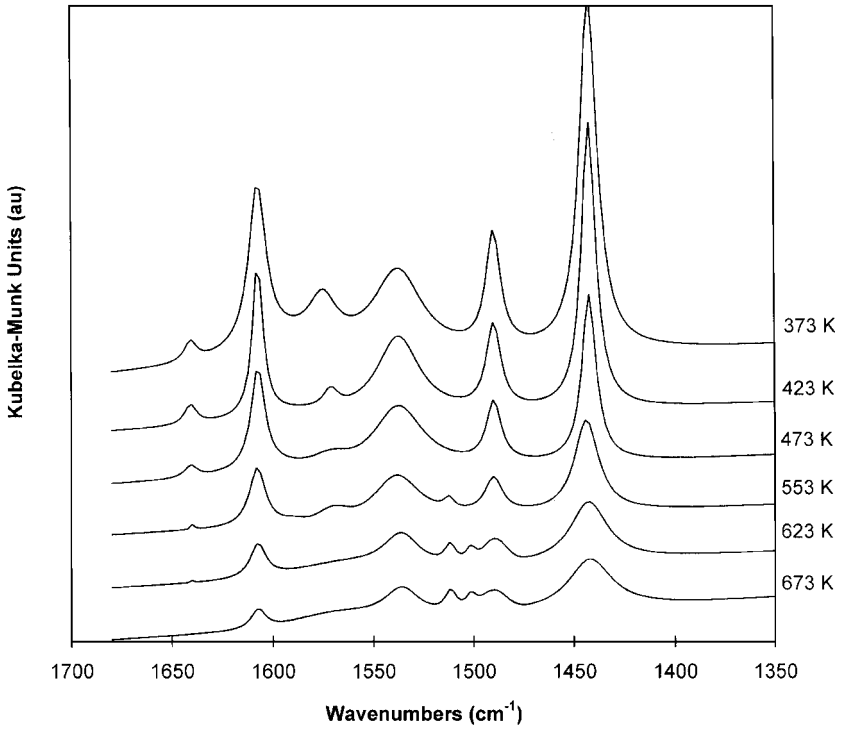

FIG. 10. *In situ* diffuse reflectance infrared (DRIFT) spectra for the co-gel, with 10 wt% W (Co-10), exposed to pyridine. Sample activated at 1073 K. Effect of heating temperature on the irreversible adsorption of pyridine on Lewis and Brønsted acid sites as a measure of the relative amount and strength of the sites.

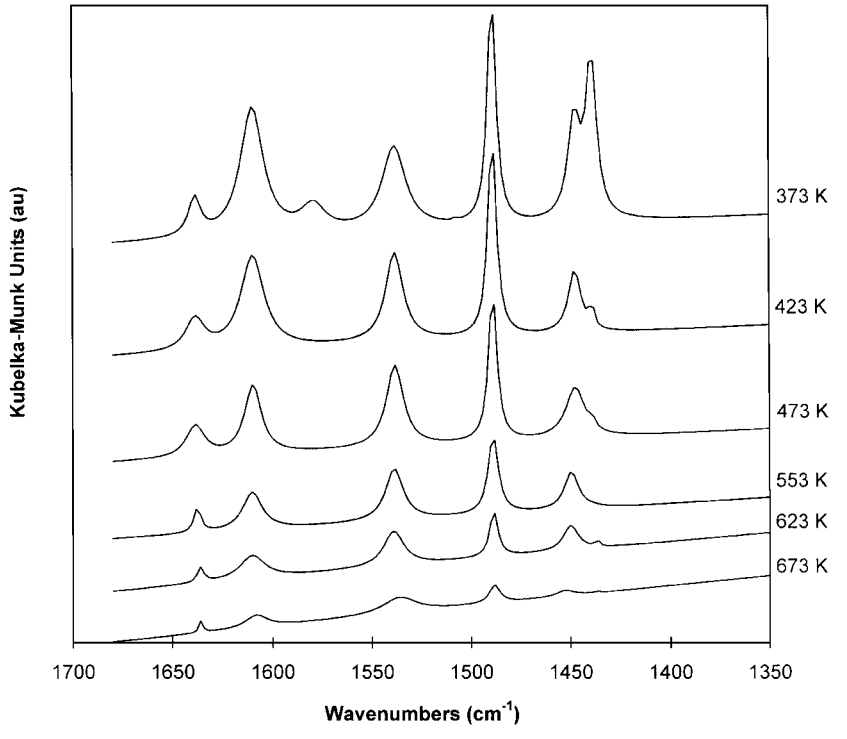

FIG. 11. *In situ* diffuse reflectance infrared (DRIFT) spectra for the co-gel, with 10 wt% W (Co-10), exposed to pyridine. Sample activated at 1223 K. Effect of heating temperature on the irreversible adsorption of pyridine on Lewis and Brønsted acid sites as a measure of the relative amount and strength of the sites.

and 1490 cm^{-1}. At temperatures of 373 and 423 K, a large peak at 1438 cm^{-1} was caused by the substantial presence of physisorbed pyridine. This peak disappeared with heating above 423 K. Two prominent features were observed in these spectra. First, the Brønsted peak at 1490 cm^{-1} was significantly larger than the Lewis peak at 1447 cm^{-1} which indicated that the surface possessed an acid site distribution of which 60–75% were Brønsted acid sites. Second, the evolution of pyridine infrared spectra showed that the peak at 1490 cm^{-1} was still evident at 623 K. This peak indicated that the Brønsted acid sites were stronger on Co-10 with activation at 1223 K because they irreversibly adsorbed pyridine at a higher temperature than Co-10 activated at 1073 K.

The acidity of Co-10 and IWP-10, with respect to activation temperature, was examined by pyridine DRIFT spectroscopy. The DRIFT spectra shown in Figs. 10 and 11 were representative of all the spectra for Co-10 and IWP-10. Table 4 gives the results of analyses of the types of acid sites on the materials and the strength of the Brønsted acid sites. Comparison of the rate of isomerization of *n*-butane to the Brønsted acidity revealed that the most active samples also possessed the highest percentage of Brønsted acid sites. Significantly, Table 4 illustrates that, although all the samples possessed Brønsted acid sites, those samples capable of adsorbing pyridine irreversibly at 623 K were also active in *n*-butane isomerization. Hence, catalytic activity correlated with the presence of stronger Brønsted acid sites.

TABLE 4

Catalytic and Acidic Properties of 10 wt% W Zirconia-Tungstate Aerogels

Sample	Activation temperature (K)	*n*-Butane isomerization activity (μmol/h/m^2)	% Brønsted acid sites of total acid sites at 473 K[a]	Adsorb pyridine, on Brønsted acid sites, irreversibly at 623 K
Co-10	1073	0.00	17	No
	1173	1.99	62	Yes
	1223	3.52	75	Yes
	1273	0.00	55	No
IWP-10	973	0.11	23	No
	1073	1.39	55	No
	1123	3.59	65	Yes
	1173	3.41	70	Yes
	1223	1.30	63	Yes

[a] Percentage Brønsted acidity given with approximately ±5% accuracy.

Infrared Signatures of Supported Tungstate

DRIFT spectroscopy was used to study the state of the surface tungstate species and made it possible to relate the surface species to the surface acidity. *Ex situ* DRIFT spectra of IWP-10 and Co-10 under ambient conditions showed a peak on both materials at 750 cm^{-1} which became more prominent with increasing activation temperature. We assigned this infrared band to a W–O vibration of surface tungstate species, possibly from both crystalline and noncrystalline species. Figures 12a, b show the *in situ* DRIFT spectra of IWP-10 in a helium atmosphere. Figure 12a contains spectra of IWP-10 at room temperature in helium before the temperature treatment. A peak was present at 970 cm^{-1} which shifted to 990 cm^{-1} with the increasing activation temperature. This peak disappeared at an activation temperature of 1173 K, corresponding to the emergence of crystalline WO_3. Previous reports have indicated that

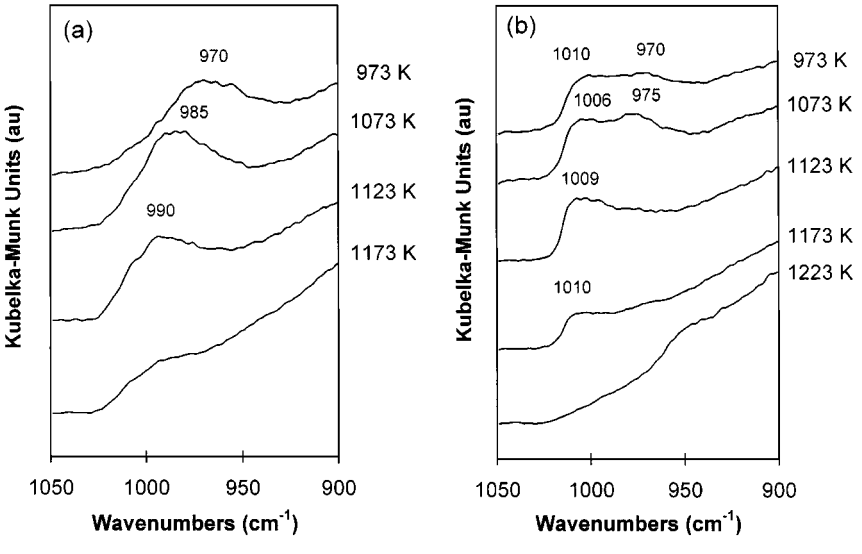

FIG. 12. *In situ* diffuse reflectance infrared (DRIFT) spectra for the impregnated aerogel, with 10 wt% W (IWP-10), in helium at (a) room temperature and (b) 588 K for 15 min. Effect of activation temperature on tungstate species present on the surface under reaction conditions.

the molecular structures of supported tungstate on zirconia follows structures observed in aqueous media. Using Raman spectroscopy, vibrations from 960 to 990 cm^{-1} have been assigned to the symmetric stretching W=O vibration of solvated polytungstate species (20). It has also been reported that octahedrally coordinated monooxo structures have similar Raman and infrared band assignments (20). Hence, we assigned the infrared bands in the range of 970 to 990 cm^{-1} to solvated polytungstate species, resembling $W_6O_{20}(OH)^{5-}$(aq), $W_{12}O_{41}^{10-}$(aq), and $W_{12}O_{39}^{6-}$(aq).

Figure 12b contains spectra of IWP-10, at 588 K in helium, under similar conditions to those of the catalytic pretreatment. A new band emerged at 1010 cm^{-1} which, by analogy to Raman band assignment, was caused by the symmetric W=O stretching vibration of a new octahedrally coordinated surface species WO_x. It is believed that upon dehydration at an elevated temperature, the hydrated surface metal oxide decomposes to form dehydrated surface oxide species. The Raman measurements of Kim *et al.* (20) were performed after treatment at 773 K under vacuum, contrasting with our conditions at 588 K in helium. Hence, the presence of two peaks at 970 and 1010 cm^{-1} was attributed to incomplete decomposition of hydrated polytungstate into a dehydrated surface structure. With a sufficiently high activation temperature of 1123 K, only the dehydrated surface structure existed as evidenced by a single peak at 1009 cm^{-1}. The presence of this single peak corresponded to the sample with the highest specific catalytic activity and indicated the importance of the surface tungstate WO_x in the isomerization of *n*-butane.

We note in passing that other factors may affect the spectroscopic vibrations of surface tungstate. In particular, interactions between potassium and tungsten oxide, due to sample dilution in KBr, could have affected the infrared signature of the surface tungstate. For example, K_2O–V_2O_5 interaction species appear at lower frequency than isolated V_2O_5 species on TiO_2 under dehydrated conditions (30). Evidence to suggest that the peak at 970–990 cm^{-1}, at 588 K in helium, was not a K_2O–WO_x interaction species associated with WO_x at 1010 cm^{-1}, was twofold: (i) a peak at 970–990 cm^{-1} also existed under ambient conditions when an interaction species was unlikely to exist between a physical mixture of KBr and zirconia-tungstate; (ii) the peak disappeared with increasing activation temperature before the surface WO_x transformed into crystalline WO_3. There was no evidence for the existence of K_2O or other factors that might affect infrared signatures.

Figure 13 shows similar *in situ* DRIFT spectra for Co-10 before and during heat treatment at 588 K in helium. The *in situ* DRIFT spectra in Fig. 13a showed a peak at 970 cm^{-1} which shifted to 990 cm^{-1} with increasing heat treatment. As was the case with IWP-10, the catalytically inactive and active samples activated at 1073 K and 1223 K, respectively, possessed peaks at 970 cm^{-1} and 990 cm^{-1}, respectively. The similar signatures of polytungstate in Co-10 and IWP-10 implied that the locations of the dopant were different, but not the state of the dopant. This observation was consistent with the same tungstate precursor, in Co-10, being entrapped in the bulk of zirconia during gel formation rather than participating in the formation of a conventional mixed oxide. Figure 13b shows the spectra of Co-10 at 588 K. The emergence of a peak in the range 1005 to 1010 cm^{-1} was also evident on each of the samples. The most active sample in *n*-butane isomerization also corresponded to the sample with only one peak present at 1008 cm^{-1} which coincided with a surface with only surface WO_x species present on

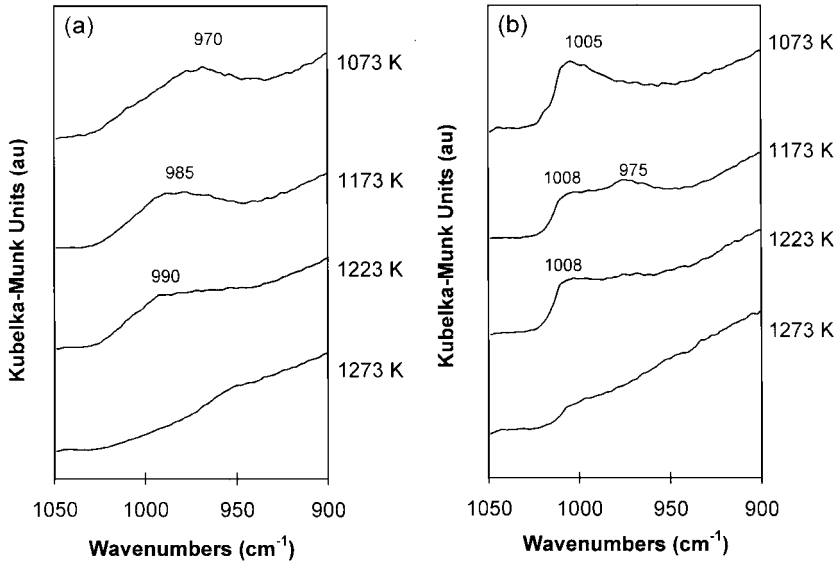

FIG. 13. *In situ* diffuse reflectance infrared (DRIFT) spectra for the co-gel, with 10 wt% W (Co-10), in helium at (a) room temperature and (b) 588 K for 15 min. Effect of activation temperature on tungstate species present on the surface under reaction conditions.

the sample. Co-10 activated at 1073 K possessed a peak at 1005 cm^{-1} but was catalytically inactive due to the requirement for tungstate to be expelled from the bulk to the surface of the aerogel. The surface-active species could only be reliably identified by an infrared band above 1008 cm^{-1}.

DISCUSSION

The aim of this study has been to determine the role of preparation on textural, structural, catalytic, and acidic properties of zirconia-tungstate aerogels. Preparative variables investigated were the preparation method, activation temperature, tungstate loading, and sol–gel parameters. The discussion below examines the influence of these variables on the final properties of the materials. A schematic model of the surface species is developed to facilitate the understanding of the relationships between these properties.

Influence of Preparation on the Textural Properties

The materials texture did not appear to affect the structural or chemical properties; therefore we discuss the relationship between preparation and texture to contribute to the understanding and design of aerogels. Several points were evident from our results: (1) Comparison of two identical co-gels with different tungstate loading, Co-10 and Co-18, demonstrated the negligible effect of loading at this level on the textural properties. (2) Comparison of two materials prepared by the same method but with different sol–gel parameters, IWP-10 and IWP-18, established that the choice of solvent played a strong role on the pore size distributions. (3) Comparison of two identical materials, save for the preparation method, IWP-18 and Co-18, illustrated that the choice of preparation method affected the pore characteristics.

Comparison of IWP-10 and IWP-18 allowed investigation of the role of the sol–gel parameters on the morphology of the final aerogel. Table 1 shows the differences between the two materials, namely the choice of solvent, water ratio, and acid ratio. The textural properties of the aerogels depend on the quality of the gel network which relies on the growth of the polymeric particles determined by the relative rates of hydrolysis and condensation in the sol–gel step (31). Large water ratios are known to favor highly condensed products by increasing the amount of partially hydrolyzed species available for condensation (25, 31). Large acid concentrations can severely retard condensation kinetics by protonation of hydroxo ligands, thus decreasing the driving force for nucleophilic substitution necessary for condensation (32). Hence, variation of either the water ratio or the acid ratio will have a significant effect on the morphology of the aerogels. However, both the water and acid ratios were increased in the preparation of IWP-18. Previous work has shown that the time of gelation is a good indicator of the relative rates of hydrolysis and condensation (25). Since IWP-10 and IWP-18 have sufficiently close gel times, 48 and 34 s, respectively, we believe that the relative rates of hydrolysis and condensation were reasonably similar. Therefore, the morphology of the two gels would be comparable for both IWP-10 and IWP-18, despite the large increases in both the hydrolysis and acid ratios (33). Table 2 and Fig. 4 illustrate the large difference in pore volumes and pore size distributions of the two materials. We conclude that the change in texture was affected by the choice of solvent.

The role of the solvent was as follows. IWP-10 and IWP-18 were prepared using 1-propanol and ethanol, respectively, but the same alkoxide precursor, zirconium *n*-propoxide. When the propoxide precursor was dissolved in ethanol, the 4-fold coordinated zirconium atom is expected to undergo coordination expansion by solvating with the ethanol solvent. Another phenomenon that may have occurred was alcohol exchange which is facilitated when the solvent is less sterically bulky than the alkoxide ligand (31). Consequently, IWP-18, prepared from a propoxide precursor, had predominately ethoxy ligands as opposed to propoxy ligands when dissolved in ethanol. In polar solvents, such as alcohol, alkoxy bridging and alcohol association may occur, producing larger oligomeric building blocks. Oligomer size is expected to increase with decreasing size of alkoxy group, implying that the preparation of IWP-18 may have involved larger initial building blocks in the formation of the alcogel. This effect has been observed for titanium alkoxides, with $Ti(OEt)_4$ exhibiting oligomeric structures in alcohol, whereas $Ti(OPr)_4$ remains monomeric (31). The significantly different pore volume of IWP-18 suggests that, despite similar gel times, changing the solvent resulted in growth of particles before alcogel formation, which in turn increased the average pore size.

Influence of Preparation on the Crystallization Behavior

We determined that the preparation method and tungstate loading played a dominant role on the structural changes of zirconia and tungsten oxide. The role of the dopant location was observed to affect the sintering behavior of zirconia. Zirconia (containing 10 wt% W) remained in a metastable tetragonal phase with activation at 1173 K and 1223 K when prepared by impregnation and co-gel routes, respectively. The higher temperature of crystal structure transformation for the co-gel demonstrated the ability of tungstate, located initially in the bulk of zirconia, at retarding the tetragonal-to-monoclinic transformation. This observation was supported by the textural results of IWP-18 and Co-18, identical materials except for dopant location. The surface areas of Co-18 and IWP-18, activated at 1073 K, were 68 and 56 m^2/g, respectively. The higher surface area of Co-18 verified the effectiveness of bulk tungstate in the retardation of sintering.

The effect of dopant loading on the crystal structure of the tungstate was considered by comparing co-gels with 10 and 18 wt% W. As stated above, the very similar surface areas and pore volumes showed that the loading did not affect the textural properties. This observation was consistent with previous reports which indicate that a surface density of 5 W-atoms/nm^2, after activation at 1073 K, is sufficient to stabilize the surface area of zirconia (11), above which no effect is observed physically. Zirconia-tungstate materials have been previously reported to be catalytically active after calcination in the range 1073 to 1123 K (10). Surface tungstate density from 1073 to 1173 K, calculated using the measured surface areas and assuming 0.16 nm^2 per W-unit, was 5.0 to 7.4 W-atoms/nm^2 which was above that required for maximum stabilization of the zirconia support (11). Saturation monolayer coverage of zirconia by tungstate is attained during calcination by sintering of the underlying zirconia support. We observed that higher calcination temperatures, in the range 1123 to 1223 K, were required for maximum specific activity in *n*-butane isomerization. Maximum catalytic activity occurred after calcination at 1123 K which corresponded to a surface density of 6.0 W-atoms/nm^2. This loading was close to theoretical monolayer coverage of approximately 6.25 W-atoms/nm^2 calculated from the spreading of a single tungsten oxide layer on a support. Actual formation of crystalline WO_3 occurred in the range 5 to 6 W-atoms/nm^2 as determined experimentally by Raman spectroscopy. Hence, we conclude that maximum specific activity was at saturation coverage of zirconia by tungstate which was approximately equal to a theoretical monolayer coverage. It was noted that saturation coverages reported in the literature have varied from 4 (21) to 5 W-atoms/nm^2 (11), contrasting with 5–6 W-atoms/nm^2 on zirconia aerogels. This higher surface density suggested that solid–solid wetting of zirconia by tungstate was more efficient, possibly due to the significant hydroxyl population of the aerogels (33).

Influence of Preparation on the Surface Tungstate Species

Several preparative variables affected the relationship between activation temperature and crystallization of tungsten oxide. The dependence of crystallization on the activation temperature was altered by the loading, which was not surprising from previous studies, and the preparation method, which was a finding of this study. Here we discuss the effect of preparative route and activation temperature on the state of surface tungstate species before crystallization into WO_3 which was undesired for isomerizing *n*-butane. The vibrational features of tungsten oxide on a solid surface have been extensively studied with Raman spectroscopy (15, 20) but less so with infrared spectroscopy. Most of the Raman studies have been made under dehydrated conditions (21), but none under *in situ* reaction conditions. As mentioned in the results section, we used DRIFT spectroscopy to characterize the surface tungstate species, in flowing helium, at room temperature and at 588 K.

DRIFT spectroscopy was used to resolve the species present under ambient conditions. We have assumed that the molecular structures of tungstate on zirconia were comparable to structures found in aqueous solution (21). In this work, we assigned the infrared bands from 960–990 cm^{-1} to W=O vibrations of hydrated polytungstate species on zirconia with structures resembling $W_6O_{20}(OH)^{5-}$, $W_{12}O_{41}^{10-}$, and $W_{12}O_{39}^{6-}$. At ambient conditions, only bands due to these hydrated polytungstate species were observed. As activation temperature increased from 973 to 1123 K, this band shifted from 970 to 990 cm^{-1}. In aqueous solution, the specific tungsten oxide species that can exist depends on the solution pH and concentration (34). Referring to the tungsten oxide aqueous phase diagram, we note that the predominant species in solution changes from $W_6O_{20}(OH)^{5-}$ to $W_{12}O_{41}^{10-}$ or $W_{12}O_{39}^{6-}$ as the ion concentration increases. We also note that the surface density of hydrated tungsten oxide on zirconia increased with the activation temperature due to sintering of the underlying zirconia support. Hence, the peak shift seen in the DRIFT spectra at ambient conditions was caused by conversion from one polytungstate species to another as surface density increased.

The influence of the surface structures on the catalytic properties was demonstrated by comparing the catalytic data for IWP-10 to the tungstate species identified by DRIFT spectroscopy at elevated temperature. Table 4 lists the catalytic activities of IWP-10 over the range of activation temperatures. Comparison with Fig. 12b shows that the infrared peak at 1010 cm^{-1}, under heated conditions, became more prominent with increasing catalytic activity. Our results showed that activity in *n*-butane isomerization correlated with the presence of an infrared peak at 1008–1010 cm^{-1}, which is indicative of an active surface tungstate species (WO_x) described in the literature as a distorted octahedrally coordinated polyanion. The sample with the highest specific activity corresponded to one with only a single peak at 1010 cm^{-1} in the *in situ* DRIFT spectra. The infrared signatures in this region disappeared upon crystallization of tungsten oxide. There also appeared to be a relationship between the infrared signatures of the tungstate species present under ambient and heated conditions. Under ambient conditions, the sample calcined at the optimum activation temperature for catalytic activity possessed a peak positioned at 990 cm^{-1}. Catalytically inactive materials could be identified by a vibrational band located at the lowest frequency of 970 cm^{-1}, making it possible to easily distinguish between potentially active and inactive materials.

By preparing samples at a variety of activation temperatures, we were able to study the evolution of zirconia-tungstate as it changed from a material inactive in the isomerization of *n*-butane into a material which was active.

Up to this point, we have shown the effect of activation temperature on surface structures and its use in the characterization of zirconia-tungstate. Further comparison of Co-10 and IWP-10 allowed us to examine the relationship between surface structures and the corresponding activity and acidity. Table 4 compares the activity and Brønsted acidity of Co-10 and IWP-10. As discussed below, both materials were active in the isomerization of *n*-butane when stronger Brønsted acid sites were present on the surface. These sites were identified by the highest temperature at which they can adsorb pyridine irreversibly as determined by infrared spectroscopy. We have already determined that the catalytic activity was related to a particular surface tungstate species. The link between catalytic activity and stronger Brønsted acidity established that the active species was responsible for the generation of stronger acid sites which resulted in catalytic activity. It was clear, however, that Co-10 and IWP-10 were catalytically active at completely different activation temperatures. We concluded that the preparative route strongly influenced the activation temperature required to produce a catalytically active material, but it did not affect the active species responsible for the activity.

Schematic Models of 10 wt% W Zirconia-Tungstate Aerogels

Figure 14 shows a model of the surface of IWP-10 at elevated temperatures to summarize the evolution of WO_3 crystallites and WO_x monolayer over all activation temperatures. Analysis of the *in situ* DRIFT spectra allowed identification of the species present on the surface during the reaction. Activation at 973 K created a material with an infrared peak at 970 cm^{-1} under ambient conditions and peaks at 970 and 1010 cm^{-1} under heated *in situ* conditions (Fig. 12). The band at 1010 cm^{-1} was attributed to an octahedrally coordinated surface species formed by decomposition of hydrated polytungstate species upon heating at elevated temperatures. Therefore, as shown in Fig. 14, IWP-10 activated at 973 K possessed a small population of dehydrated surface tungstate, denoted as WO_x, while the leftover tungstate remained in the original polytungstate state. When the activation temperature was increased from 973 to 1073 K, two peaks were detected at 970 and 1010 cm^{-1} under *in situ* reaction conditions. This behavior was again ascribed to partial decomposition of hydrated polytungstate into a dehydrated surface structure as shown in the model. Finally, Fig. 14 illustrates that activation at 1123 K yielded the most active material corresponding to one with the highest coverage of zirconia by the active surface tungstate species WO_x. Crystalline WO_3 was also present, as identified by Raman spectroscopy, and proceeded to completely cover the surface with the higher activation temperature. In this schematic model, the growth of WO_3 crystallites does not imply the displacement of the WO_x monolayer because the bottom of each crystallite is in essence a surface phase interacting with the support. A similar model of the surface of Co-10 is given in Fig. 15. In this case, however, tungstate was present in the bulk of the material resulting in the surface structure being highly sensitive to the activation temperature. At 1073 K, the material was inactive, implying that the active WO_x surface species was not present. DRIFT spectroscopy at ambient conditions suggested that hydrated polytungstate was evident by a peak at 970 cm^{-1} in Fig. 13. Activation at 1173 K caused the expulsion of tungstate from the bulk of zirconia, which was capable of partially decomposing from hydrated polytungstate into WO_x upon heating at 553 K. Higher temperature activation resulted in complete coverage of zirconia by surface tungstate and tungsten oxide, followed by further crystallization of WO_3.

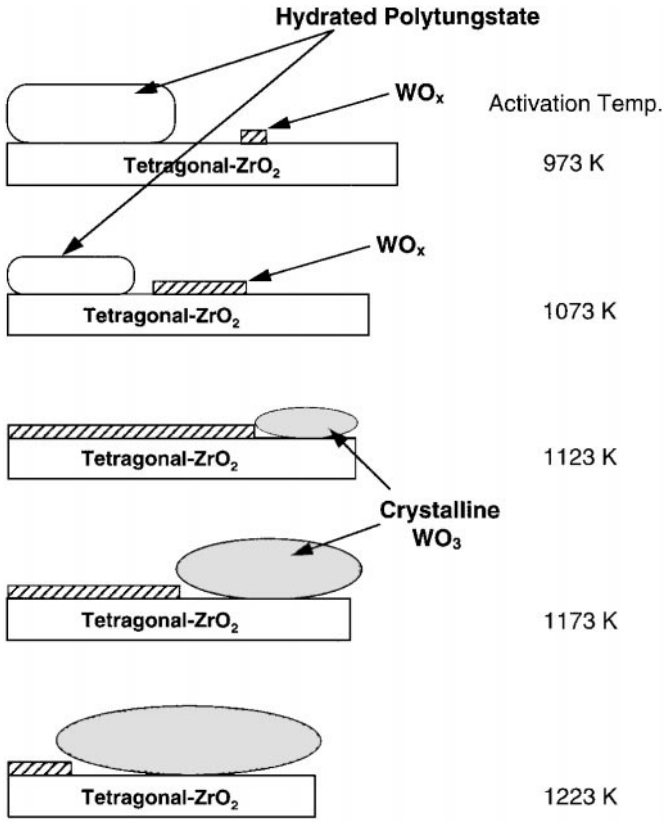

FIG. 14. Schematic model of IWP-10 at 553 K in helium.

Brønsted Acid Strength Hierarchy in Zirconia-Tungstate Aerogels

In this work, we characterized the acidic properties of zirconia-tungstate aerogels by the irreversible adsorption of pyridine as the pyridinium ion. Spectroscopic analysis of adsorbed pyridine allowed a noncontroversial technique to rank Brønsted acid strength—stronger Brønsted acid sites retain adsorbed pyridine at higher temperatures (35). We also used the isomerization of *n*-butane as a probe for acidity because it is generally accepted to be the most useful

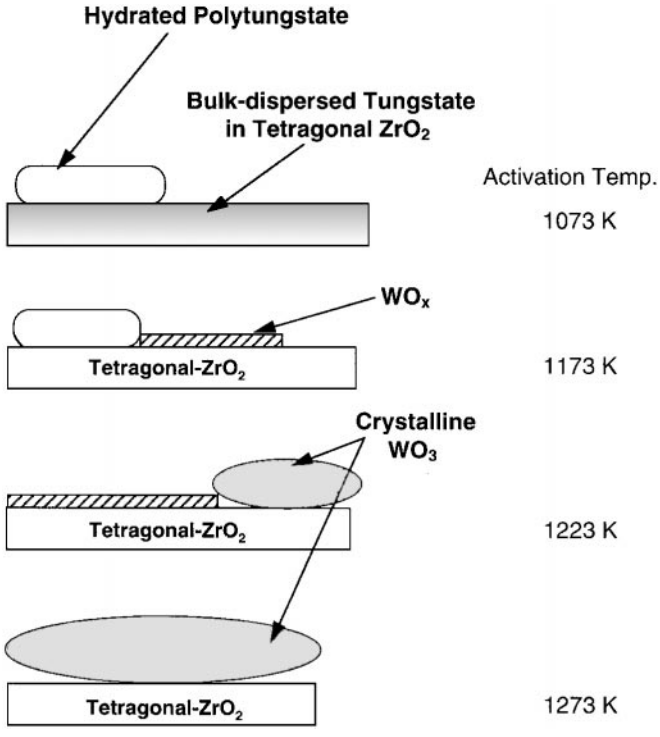

FIG. 15. Schematic model of Co-10 at 553 K in helium.

in the screening of catalytic materials and is known to require very strong Brønsted acid sites (3). Before arranging an acidity scale to rank Brønsted acid strengths, we verified that the catalytic reaction was indeed a probe for very strong acid sites. Table 4 makes evident that all Co-10 samples capable of catalyzing *n*-butane isomerization also adsorbed pyridine at 623 K. It illustrates that inactive samples only retained pyridine up to a temperature of 553 K. This established a correlation between the catalytic activity and the presence of stronger Brønsted acid sites on the surface and verified the use of the isomerization as a probe reaction for acid sites of a certain strength. Exact placement of the isomerization in an acidity scale was accomplished by referring to IWP-10 activated at 1073 K. It was noted that some activity was detected in the isomerization of *n*-butane but adsorbed pyridine was *not* detected at 623 K. We concluded that irreversible adsorption of pyridine at 623 K required slightly stronger acid sites than those that were involved in *n*-butane isomerization at 553 K.

To summarize, Fig. 16 illustrates a hierarchy of Brønsted acid strengths accessible by zirconia-tungstate aerogels. The rank order of Brønsted acid strengths was based on activity in *n*-butane isomerization and the temperatures at which samples irreversibly adsorbed pyridine. A similar, but slightly less developed, acidity scale has been used to qualitatively describe the acidity of zirconia-silica-sulfate, zirconia-sulfate, and zirconia aerogels (24). In this work, it was possible to separate zirconia-tungstate into three regimes of increasing Brønsted acid strength: (i) samples capable of adsorbing pyridine irreversibly at 553 K; (ii) samples capable of *n*-butane isomerization at 553 K, and (iii) samples capable of adsorbing pyridine irreversibly at 623 K. In doing so, we have shown that the Brønsted acid strength, and thus the catalytic activity in *n*-butane isomerization, is dependent on the preparation method and activation temperature.

Figure 17 relates the acidity of the zirconia-tungstate to zirconia aerogels modified by a range of other dopants. The same chemical probes, alkane isomerizations, and base adsorption, were used to describe the Brønsted acid strengths

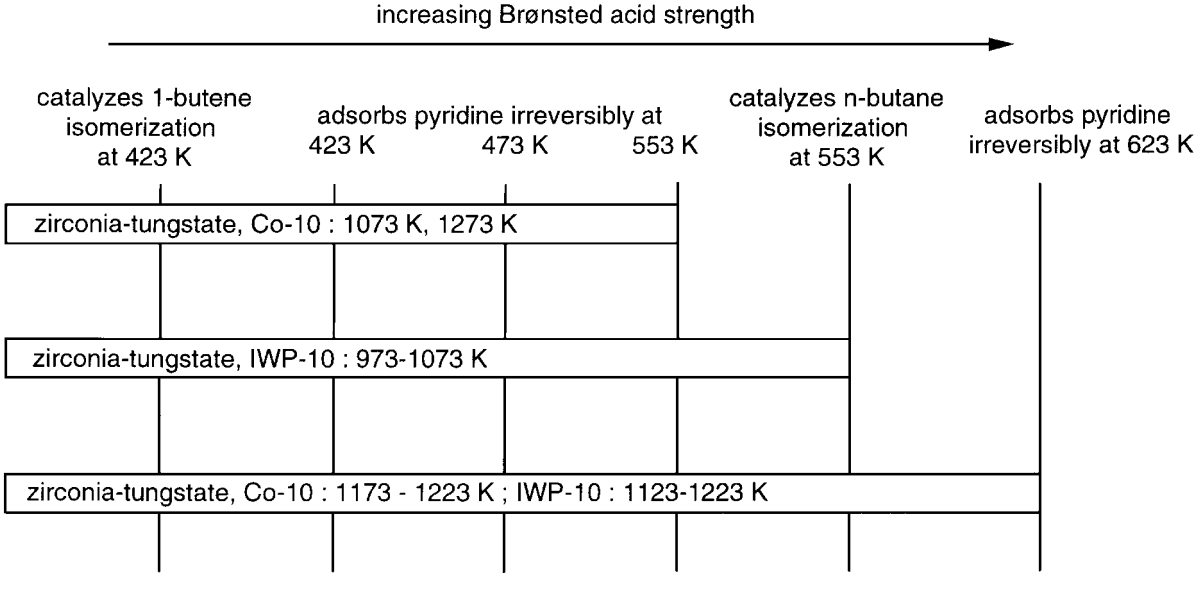

FIG. 16. Brønsted acid hierarchy in zirconia-tungstate aerogels. Activation temperatures required for a given acid strength displayed in bars.

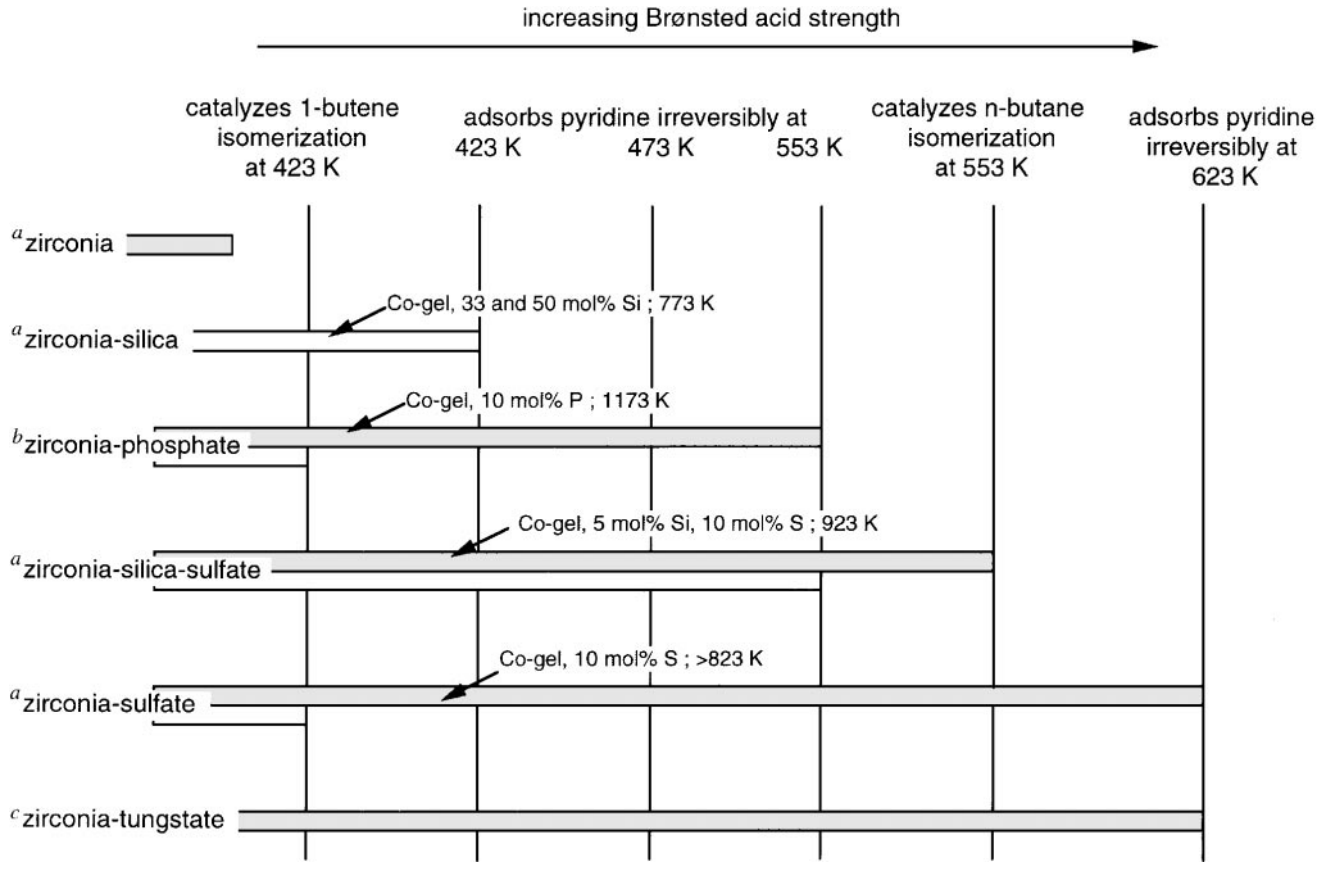

FIG. 17. Brønsted acid hierarchy in modified zirconia aerogels. Dopant content and activation temperatures appear above bars. Shaded bars represent materials after optimal activation. Open bars represent materials activated at 773 K.

of zirconia promoted with silica, sulfate (4), silica-sulfate (24), and phosphate (8). Figure 17 illustrates that doped zirconias after optimal high temperature activation, for enhancement of strong acid sites, usually differ from those activated at a specific temperature such as 773 K. Referring to the literature (8, 24), and to recent work with zirconia promoted with sulfate and phosphate (36), has allowed the samples after optimal activation to be accurately placed in this acidity scale. For example, for a zirconia-phosphate co-gel with 10 mol% P, we have previously established that increasing the activation temperature results in a corresponding increase in the Brønsted acid strength (8). Figure 17 shows that activation at 773 K (the open bar) produces a zirconia-phosphate co-gel active in the isomerization of 1-butene, while optimal activation at 1173 K (the shaded bar) produces a sample that can also adsorb pyridine at 553 K. Similarly, we see that zirconia promoted with sulfate or silica-sulfate can possess Brønsted acid sites of different strengths depending on the activation temperature (24). Hence, meaningful comparisons between the effects of a set of dopants on the acidity of a support must be done for optimally activated samples. Following this approach, we conclude that the rank order for the four dopants is tungstate $\sim$ sulfate $>$ phosphate $>$ silica, in terms of their ability to enhance the Brønsted acid strength of zirconia. Work is ongoing in our laboratory to develop a finer scale that could distinguish between tungstate and sulfate. Finally, Fig. 17 demonstrates that placement of other solid acids into this scale will provide a useful tool for catalyst designers in the development of acid catalysts for a specific application.

CONCLUSIONS

We have illustrated how a one-step preparation of zirconia-tungstate aerogels has allowed a deeper understanding of the relationships between preparation, structure, and acidity. Comparison of aerogels prepared by a one-step and an incipient wetness preparation has shown that the optimum activation temperature in *n*-butane isomerization strongly depends on the method of preparation. Specifically, the tungstate dopant contained in the bulk of the co-gel required expulsion onto the surface of zirconia before the onset of activity. This demonstrated the dependence of the calcination temperature for catalytic activity on the location of the dopant. The active sites in this reaction were

determined by DRIFT spectroscopy to be identical regardless of preparative method. They correspond to an octahedrally coordinated surface tungstate species. Our results further elucidate the relationship between surface acidity and catalytic activity. Maximum catalytic activity occurred on a material with (i) a larger population of Brønsted acid sites and (ii) the presence of stronger Brønsted acid sites.

Analysis of zirconia-tungstate aerogels has also demonstrated the effectiveness of pyridine adsorption and catalytic reactions in the acid characterization of oxides. The results have allowed development of an acidity scale that can be extended to other materials. This approach will enable characterization of the maximum strength of Brønsted acid sites and provide a first step towards the development of solid acids for a specific application by design.

ACKNOWLEDGMENT

This work is supported by the Division of Chemical Sciences, Office of Basic Energy Sciences, Office of Energy Research, U.S. Department of Energy (Grant DE-FG02-93ER14345).

REFERENCES

1. Baiker, A., and Kijenski, J., *Catal. Today* **5**, 1 (1989).
2. Tanabe, K., Misono, M., Ono, Y., and Hattori, H., "New Solid Acids and Bases," Elsevier Science, Amsterdam, 1989.
3. Arata, K., *Adv. Catal.* **37**, 165 (1990).
4. Ward, D. A., and Ko, E. I., *J. Catal.* **150**, 18 (1994).
5. Venkatesh, K. R., Hu, J., Dogan, C., Tierney, J. W., and Wender, I., *Energy and Fuels* **9**, 888 (1995).
6. Kustov, L. M., Kazansky, V. B., Figueras, F., and Tichit, D., *J. Catal.* **150**, 143 (1994).
7. Adeeva, V., deHaan, J. W., Janchen, J., Lei, G. D., Schunemann, V., van de Ven, L. J. M., Sachtler, W. M. H., and van Santen, R. A., *J. Catal.* **151**, 364 (1995).
8. Boyse, R. A., and Ko, E. I., *Catal. Lett.* **38**, 225 (1996).
9. Hino, M., and Arata, K., *J. Chem. Soc., Chem. Commun.*, 1259 (1987).
10. Hino, M., and Arata, K., *in* "Proc. 9th Int. Congr. Catal., 1988," p. 1727.
11. Iglesia, E., Barton, D. G., Soled, S. L., Miseo, S., Baumgartner, J. E., Gates, W. E., Fuentes, G. A., and Meitzner, G. D., *in* "Proc. 11th Int. Congr. Catal., 1996," p. 533.
12. Larsen, G., Lotero, E., and Parra, R. D., *in* "Proc. 11th Int. Congr. Catal., 1996," p. 543.
13. Soled, S. L., Gates, E., and Iglesia, E., U.S. Patent 5,422,327, 1995.
14. Chang, C. D., Kresge, C. T., Santiesteban, J. G., and Vartuli, J. C., U.S. Patent 5,510,309, 1996.
15. Meijers, S., Gielgans, L. H., and Ponec, V., *J. Catal.* **156**, 147 (1995).
16. Engweiler, J., Harf, J., and Baiker, A., *J. Catal.* **159**, 259 (1996).
17. Kim, D. S., Ostromecki, M., and Wachs, I. E., *Catal. Lett.* **33**, 209 (1995).
18. Larsen, G., Raghavan, S., Marquez, M., and Lotero, E., *Catal. Lett.* **37**, 57 (1996).
19. Zhao, B., Xu, X., Gao, J., Fu, Q., and Tang, Y., *J. Raman Spectrosc.* **27**, 549 (1996).
20. Kim, D. S., Ostromecki, M., and Wachs, I. E., *J. Mol. Catal. A: Chem.* **106**, 93 (1996).
21. Deo, G., and Wachs, I. E., *J. Phys. Chem.* **95**, 5889 (1991).
22. Afanasiev, P., Geantet, C., Breysse, M., Coudurier, G., and Vedrine, J., *J. Chem. Soc. Faraday Trans.* **90**, 193 (1994).
23. Ramis, G., Busca, G., and Lorenzelli, V., *in* "Structure and Reactivity of Surfaces," p. 777, Elsevier Science, Amsterdam, 1989.
24. Miller, J. B., and Ko, E. I., *Chem. Eng. J.* **64**, 273 (1996).
25. Ward, D. A., and Ko, E. I., *Chem. Mater.* **5**, 956 (1993).
26. Parry, E. P., *J. Catal.* **2**, 371 (1963).
27. Basila, M. R., and Kantner, T. R., *J. Phys. Chem.* **70**, 1681 (1966).
28. Ko, E. I., Bafrali, R., Nuhfer, N. T., and Wagner, N. J., *J. Catal.* **95**, 260 (1985).
29. Chan, S. S., Wachs, I. E., Murrell, L. L., and Dispenziere, N. C., Jr., *J. Catal.* **92**, 1 (1985).
30. Deo, G., and Wachs, I. E., *J. Catal.* **148**, 335 (1994).
31. Brinker, C. J., and Scherer, G. W., "Sol–Gel Science: The Physics and Chemistry of Sol–Gel Processing," Academic Press, Boston, 1990.
32. Livage, J., Henry, M., and Sanchez, C., *Prog. Solid State Chem.* **18**, 259 (1988).
33. Ward, D. A., Ph.D. thesis dissertation, Carnegie Mellon University, 1995.
34. Baes, C. F., Jr., and Mesmer, R. E., *in* "The Hydrolysis of Cations," p. 258, Wiley, New York, 1970.
35. Bourdillon, G., Gueguen, C., and Guisnet, M., *Appl. Catal.* **61**, 123 (1990).
36. Boyse, R. A., and Ko, E. I., unpublished results.